Обзор ArXiv/astro-ph, 30 ноября – 4 декабря 2020

От Сильченко О.К.

ArXiv: 2012.01431

What does (not) drive the variation of the low-mass end of the stellar initial mass function of early-type galaxies

MUSE Paintbox II

C. E. Barbosa[1,⋆], C. Spiniello[2,3], M. Arnaboldi[4], L. Coccato[4], M. Hilker[4], and T. Richtler[5]

[1] Universidade de São Paulo, IAG, Departamento de Astronomia, Rua do Matão 1226, São Paulo, SP, Brazil
[2] Department of Physics, University of Oxford, Denys Wilkinson Building, Keble Road, Oxford OX1 3RH, UK
[3] INAF, Osservatorio Astronomico di Capodimonte, Via Moiariello 16, 80131, Naples, Italy
[4] European Southern Observatory, Karl-Schwarzschild-Straße 2, 85748, Garching, Germany
[5] Departamento de Astronomia, Universidad de Concepción, Concepción, Chile

Received October 30, 2020; Accepted December 1, 2020

ABSTRACT

Context. The stellar initial mass function (IMF) seems to be variable and not universal, as argued in the literature in the last three decades. Several relations among the low-mass end of the IMF slope and other stellar population, photometrical or kinematical parameters of massive early-type galaxies (ETGs) have been proposed, but a consolidated agreement on a factual cause of the observed variations has not been reached yet.

Aims. We investigate the relations between the IMF and other stellar population parameters in NGC 3311, the central galaxy of the

Лирика: по каким линиям определяют наклон IMF?

- NaI: сначала 8192 A, а теперь уже шире, от NaD до 2 мкм. [Na/Fe]=+0.5-+0.7!
- TiO (6120 A)
- Полоса Wingford
- Full-fitting

Что на самом деле коррелирует?

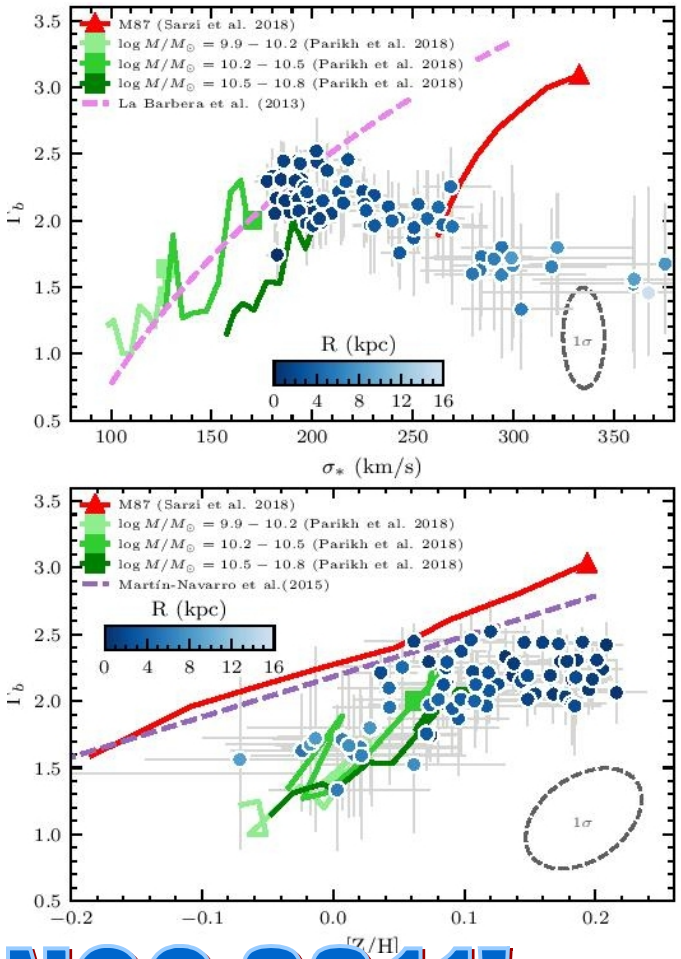

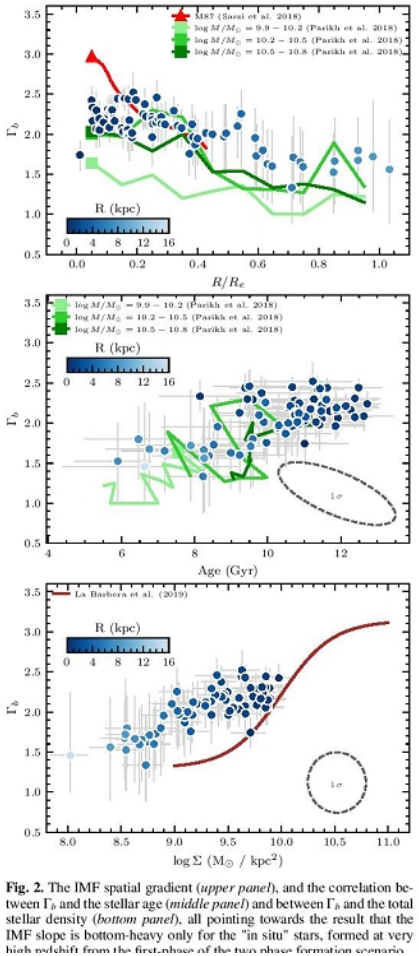

Fig. 2. The IMF spatial gradient (*upper panel*), and the correlation between Γ_b and the stellar age (*middle panel*) and between Γ_b and the total stellar density (*bottom panel*), all pointing towards the result that the IMF slope is bottom-heavy only for the "in situ" stars, formed at very high redshift from the first-phase of the two phase formation scenario.

NGC 3311!

В центре - red nugget

Камень в full-fitting: их alpha-элементы не имеют отношения к магнию

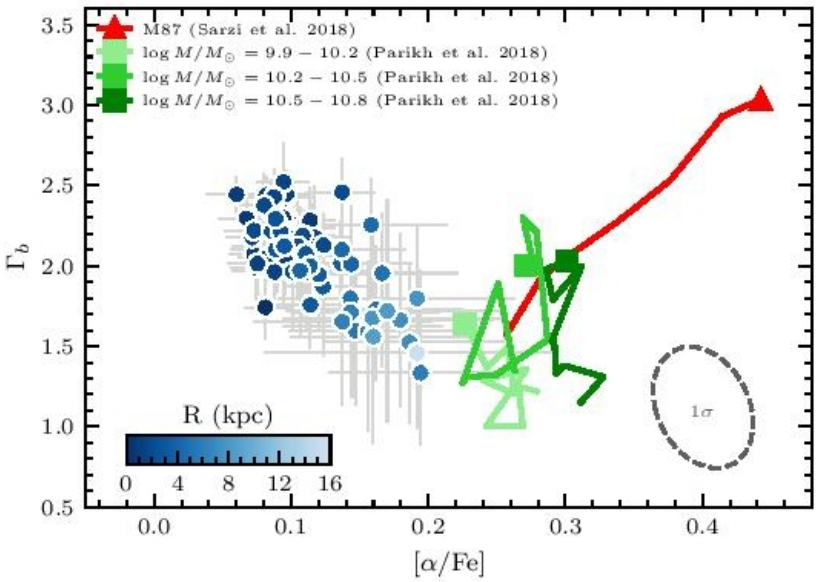

Fig. 3. IMF slope - [α/Fe] relation. For NGC 3311 (blue points) these two quantities are anti-correlated. This is the opposite of what happens for M87 (red). However, we stress that in B20 we used full-spectral fitting, rather than line-indices as in Sarzi et al. (2018) for M87, thus measuring a different quantity (from indices one is much more sensitive to Mg than to the "bulk" changes in all α elements). Note that the [α/Fe] estimates obtained in Barbosa et al. (2018) from the same data but using line-indices imply a high value, which would shift the blue data-points towards the red and green lines. The situation is much more complicated for the results based on MaNGA (green lines) where different galaxies, with possibly different [α/Fe] profiles are stacked together.

ArXiv: 2011.13942

Fast-spinning bars in the ΛCDM cosmological paradigm

Francesca Fragkoudi*[1], Robert J. J. Grand[1], Ruediger Pakmor[1], Volker Springel[1], Simon D. M. White[1], Federico Marinacci[2], Facundo A. Gomez[3,4] & Julio F. Navarro[5]

[1]*Max-Planck-Institut für Astrophysik, Karl-Schwarzschild-Str. 1, 85741 Garching, Germany*
[2]*Department of Physics and Astronomy, University of Bologna, via Gobetti 93/2, I-40129 Bologna, Italy*
[3]*Instituto de Investigacion Multidisciplinar en Ciencia y Tecnología, Universidad de La Serena, Raul Bitrán 1305, La Serena, Chile*
[4]*Departamento de Astronomía, Universidad de La Serena, Av. Juan Cisternas 1200 Norte, La Serena, Chile*
[5]*Department of Physics and Astronomy, University of Victoria, Victoria, BC, V8P 5C2, Canada*

The angular velocity with which galactic bars rotate is intimately linked to the amount of dark matter in the inner regions of their host galaxies. In particular, dark matter haloes act to slow down bars via torques exerted through dynamical friction. Observational studies of barred galaxies tend to find that bars rotate fast, while hydrodynamical cosmological simulations of galaxy formation and evolution in the ΛCDM framework have previously found that bars slow down excessively. This has led to a growing tension between fast bars and the ΛCDM cosmological paradigm. In this study we use a suite of state-of-the-art, high resolution, cosmological zoom-in simulations of galaxy formation and evolution to show that

AURIGA! А всего 30 галактик

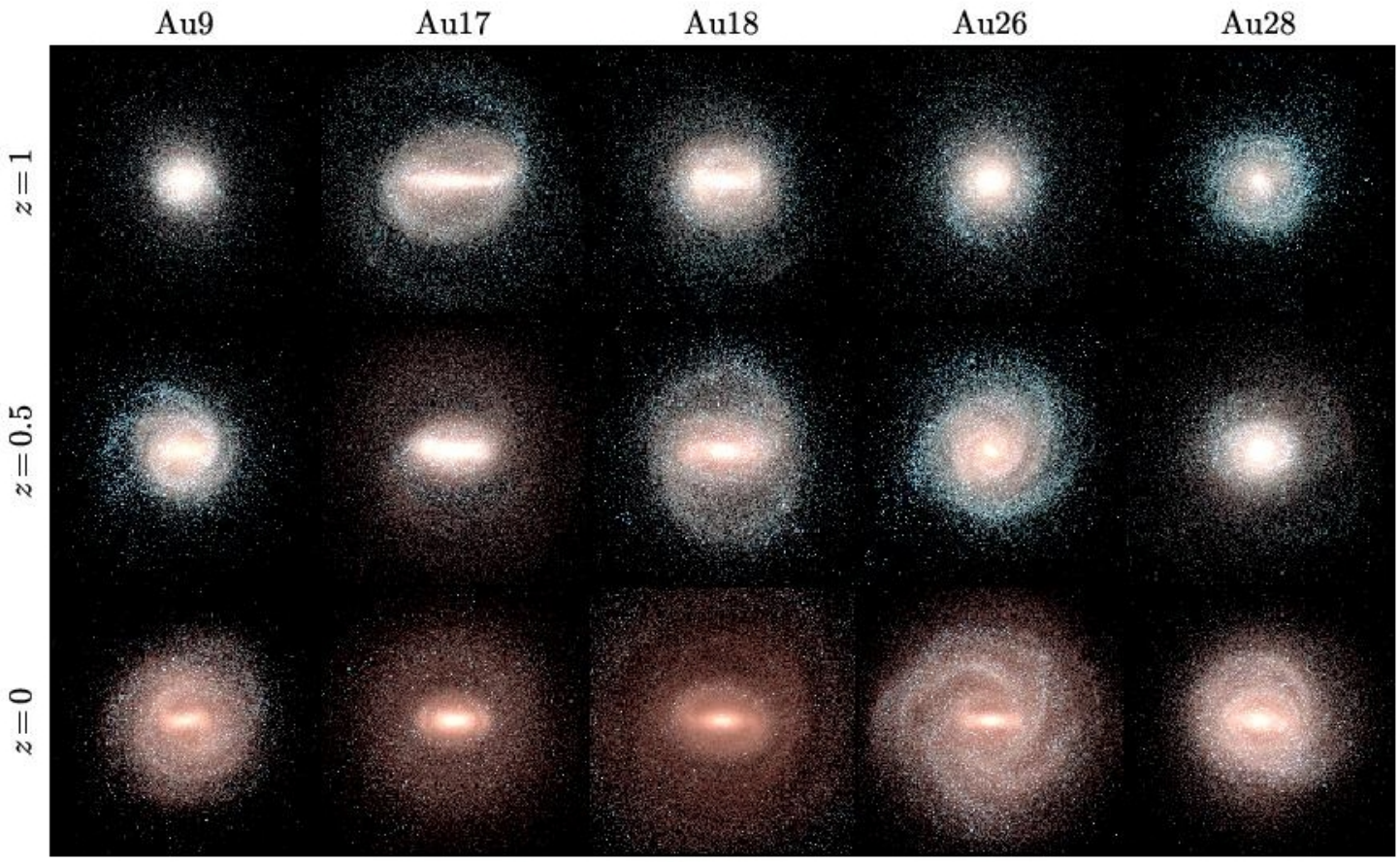

Figure 1: **Face-on projections of five Auriga barred galaxies at different redshifts:** From top

В основном, бары не замедляются

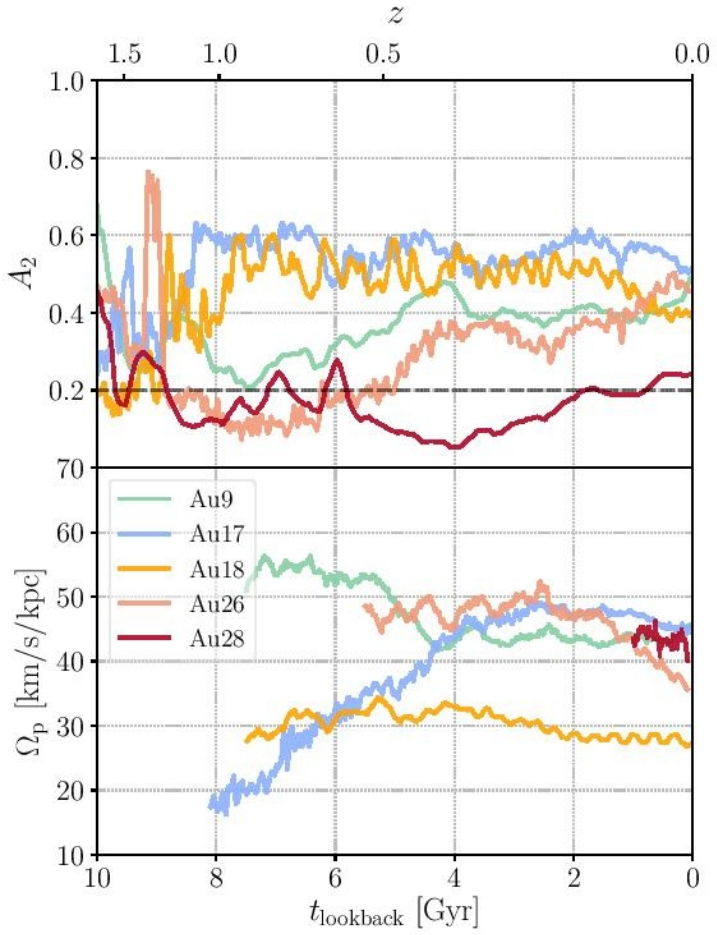

И они-таки быстрые, как в жизни

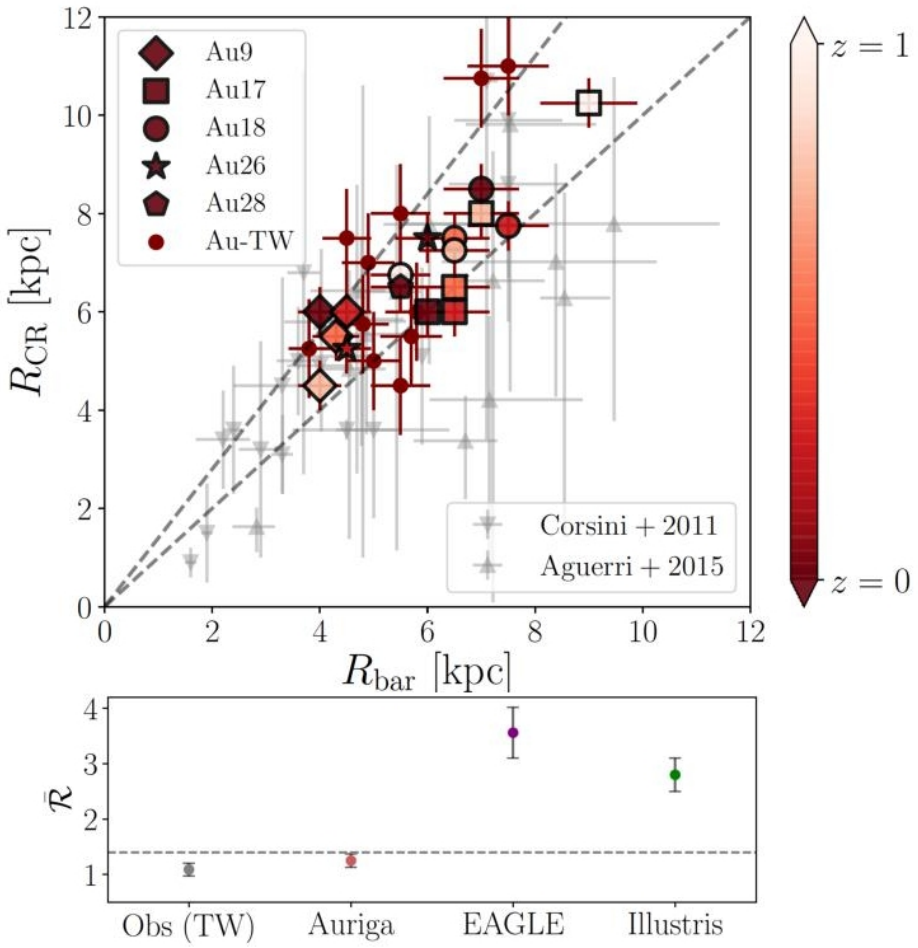

Это оттого, что много барионов – как в SPARC-галактиках

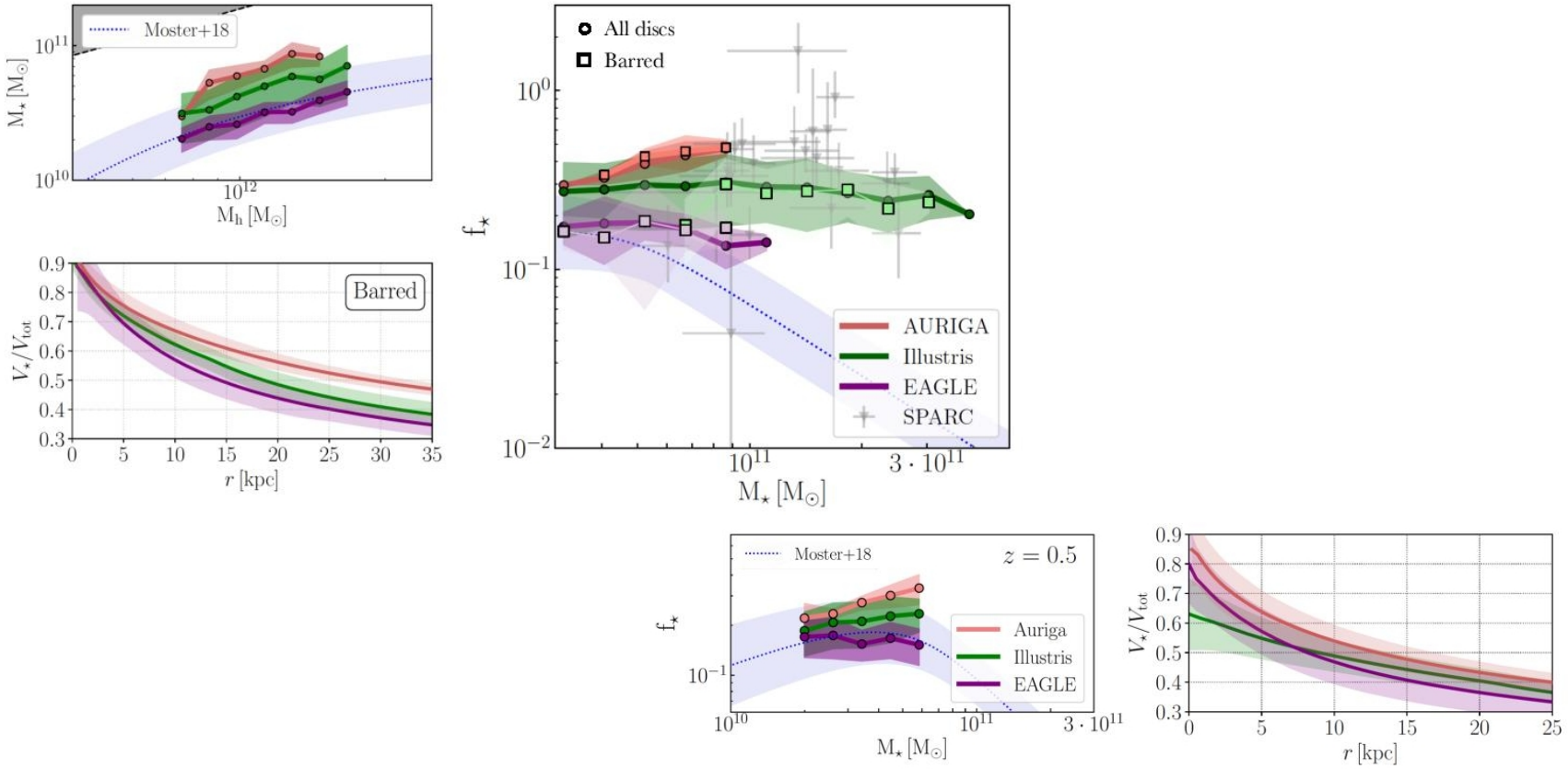

Figure 5: **Stellar to dark matter ratios at higher redshifts:** *Left:* $f_\star$ vs. $M_\star$ for Auriga, EAGLE and Illustris disc galaxies at $z = 0.5$. The dotted blue line denotes the relation determined using abundance matching and the shaded region denotes the 1σ scatter around the relation. *Right:* $V_\star/V_{\rm tot}$ for the galaxies shown in the left panel. Auriga is more baryon-dominated than EAGLE and Illustris already at higher redshifts.

Удивительная эта AURIGA!

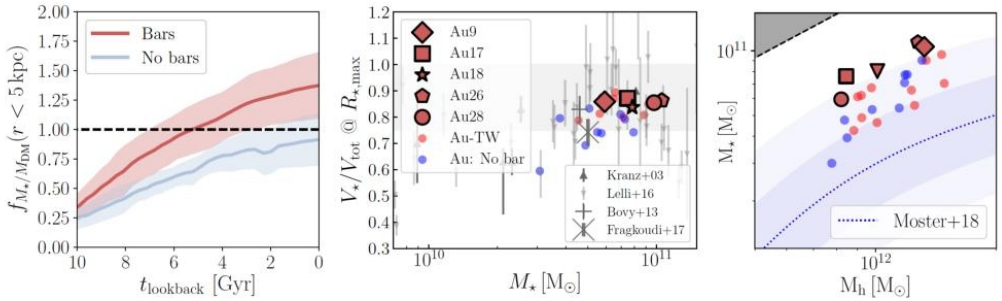

Figure 8: **Barred and unbarred galaxies in Auriga:** *Left:* ratio of stellar to dark matter mass within 5 kpc for the barred (red) and unbarred sample (blue) – see text for the definition of the samples. *Middle:* Disc maximality measured at the peak of the stellar contribution as a function of stellar mass for the Auriga barred galaxies compared to values for various galaxies in the literature. *Right:* Barred and unbarred galaxies in relation to the abundance matching relation of Moster et al. (2018). The Auriga galaxies lie $\sim 2\sigma$ above the abundance matching relation (1 and 2σ are indicated by the dark and light bands respectively). According to their calculated standard scores (or z-scores), the barred sample in this mass range has an $M_\star$ which is on average 20% higher than in the unbarred sample.

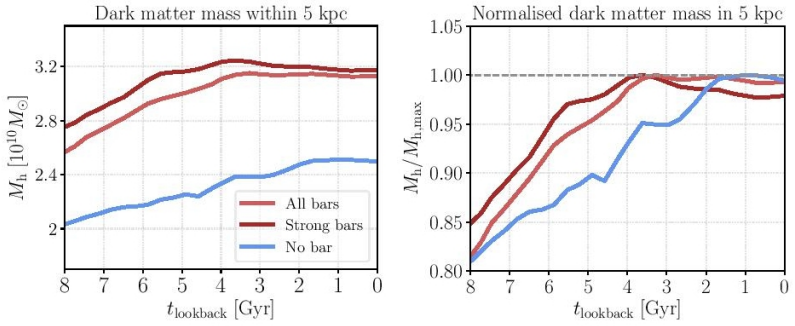

Figure 9: **Evolution of the dark matter content in the inner regions of Auriga galaxies:** *Left:* Mean enclosed dark matter mass within 5 kpc for all bars in our sample (red), for strong bars, i.e. $A_2 > 0.4$ (brown) and for unbarred galaxies (blue). *Right:* Relative dark matter content within 5 kpc for the aforementioned samples, normalised by the maximum value of the dark matter content within 5 kpc.

ArXiv: 2012.00770

Most of the cool CGM of star-forming galaxies is not produced by supernova feedback

Andrea Afruni,[1]★ Filippo Fraternali,[1] Gabriele Pezzulli[1,2]
[1]*Kapteyn Astronomical Institute, University of Groningen,Landleven 12, 9747 AD Groningen, The Netherlands*
[2] *Department of Physics, ETH Zürich, Wolfgang-Pauli-Strasse 27, 8093 Zürich, Switzerland*

Accepted XXX. Received YYY; in original form ZZZ

ABSTRACT
The characterization of the large amount of gas residing in the galaxy halos, the so called circumgalactic medium (CGM), is crucial to understand galaxy evolution across cosmic time. We focus here on the the cool ($T \sim 10^4$ K) phase of this medium around star-forming galaxies in the local universe, whose properties and dynamics are poorly understood. We developed semi-analytical parametric models to describe the cool CGM as an outflow of gas clouds from the central galaxy, as a result of supernova explosions in the disc (galactic wind). The cloud motion is driven by the galaxy gravitational pull and by the interactions with the hot ($T \sim 10^6$ K) coronal gas. Through a bayesian analysis, we compare the predictions of our models with the data of the COS-Halos and COS-GASS surveys, which provide accurate kinematic information of the cool CGM around more than 40 low-redshift star-forming galaxies, probing distances up to the galaxy virial radii. Our findings clearly show that a supernova-driven outflow model is not suitable to describe the dynamics of the cool circumgalactic gas. Indeed, to reproduce the data, we need extreme scenarios, with initial outflow velocities and mass loading factors

COS-Halo и COS-GASS: 40 спиральных галактик

(1)	(2)	(3)	(4)	(5)	(6)	(7)	(8)	(9)
Galaxy ID	z	$\log(M_*/M_\odot)$	SFR ($M_\odot$ yr^{-1})	$n_{\rm comp}$	$x_{\rm los}$ (kpc)	$y_{\rm los}$ (kpc)	$R_{\rm d}$ (kpc)	i (°)
3936	0.0441	10.1	3.98	2	38	99	2.6	65
20042	0.0468	10.0	2.51	1	-130	-146	1.6	49
8634	0.0464	10.1	0.20	1	-97	-34	0.6	25
23457	0.0354	10.1	0.25	1	76	-158	2.8	82
29871	0.0342	10.2	3.16	1	-230	-27	3.0	61
38018	0.0297	10.1	0.40	1	-32	-156	2.9	84
42191	0.0320	10.1	2.00	1	-232	72	0.7	49
41869	0.0414	10.1	3.16	3	83	103	2.0	68
170_9	0.3557	10.0	3.04	2	-33	-33	1.9	20
274_6	0.0252	9.9	0.64	2	13	31	3.2	36
359_16	0.1661	10.2	1.37	1	-13	44	3.0	38
236_14	0.2467	10.0	5.68	2	-25	58	3.7	32
168_7	0.3185	10.2	3.42	3	29	-9	4.5	36
289_28	0.1924	10.1	1.99	2	-43	92	2.1	37
126_21	0.2623	10.1	5.56	2	-74	-65	3.4	44
232_33	0.2176	10.1	2.60	2	-88	96	2.3	48
88_11	0.1893	10.1	4.18	1	27	-31	3.7	44
8096	0.0345	10.3	1.58	1	-83	158	2.1	59
32907	0.0349	10.5	0.63	-	204	-78	2.8	80
23419	0.0400	10.4	2.51	1	-48	132	2.4	70
49433	0.0458	10.5	1.58	2	231	25	1.9	40
50550	0.0350	10.3	1.99	1	158	121	1.8	52
13159	0.0437	10.4	0.40	2	100	-27	1.9	75
51025	0.0450	10.3	0.79	1	-47	214	2.3	74
41743	0.0462	10.5	1.99	2	-57	-218	2.7	69
28365	0.0321	10.4	6.3	1	124	-27	4.3	29
34_36	0.1427	10.4	14.12	2	12	-114	3.7	49
106_34	0.2284	10.5	4.52	1	61	-108	3.7	19
94_38	0.2221	10.5	4.38	4	-204	-13	4.1	59
349_11	0.2142	10.5	0.62	1	32	23	3.7	37
132_30	0.1792	10.3	11.36	1	110	-7	3.1	12
55745	0.0278	10.9	3.98	1	-16	-62	6.6	35
22822	0.0270	10.6	1.58	1	228	-96	1.8	64
55541	0.0429	10.6	3.16	1	-120	194	3.9	81
5701	0.0422	10.7	0.63	1	141	-141	2.1	31
48604	0.0334	10.6	0.40	2	-117	-90	2.2	50
48994	0.0322	10.7	1.99	1	79	-74	6.7	86
13074	0.0486	10.9	3.16	2	176	-98	3.5	71
157_10	0.2270	10.7	6.04	3	33	-12	3.1	25
97_33	0.3218	10.6	7.42	1	23	-197	5.7	61
68_12	0.2024	10.8	18.96	2	-44	-15	6.8	30

Table 1. Properties of the galaxies in our sample. (1) galaxy ID; (2) redshift; (3) stellar mass; (4) star formation rate; (5) number of kinematic components identified in the quasar spectrum (from Tumlinson et al. 2013; Borthakur et al. 2015); (6) and (7) x and y coordinates of the line of sight with respect to the galactic disc; (8) stellar disc scalelength; (9) inclination.

Что будут подгонять…

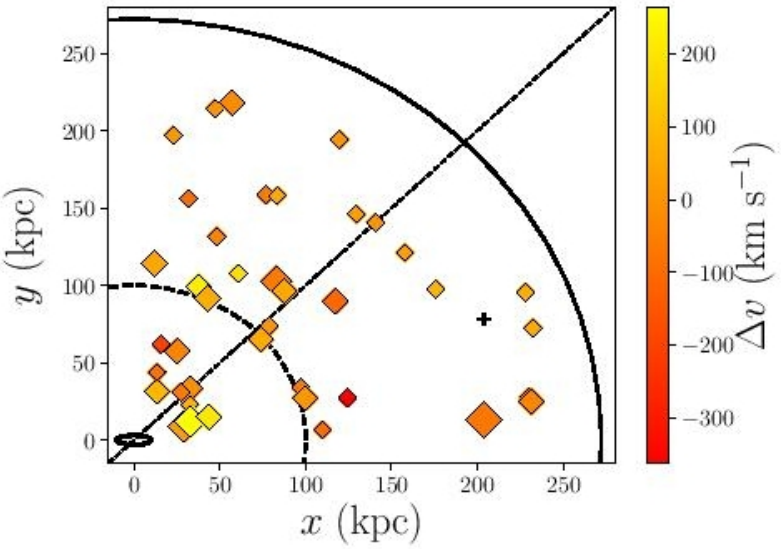

Figure 1. Plane of the observations for our subsample of galaxies taken from the COS-Halos and COS-GASS surveys. The ellipse at the bottom left corner represents the central disc galaxy, while the symbols depict the QSO lines of sight, placed at their corresponding distance from the central object, with the black cross representing the non-detection. The colorbar shows the average velocity of the cool CGM found for each sightline, while the size of the symbols is related to the number of components identified in each spectrum. The black solid curve represents the median virial radius of our galaxy sample (272 kpc), while the dashed curve represents a radius of 100

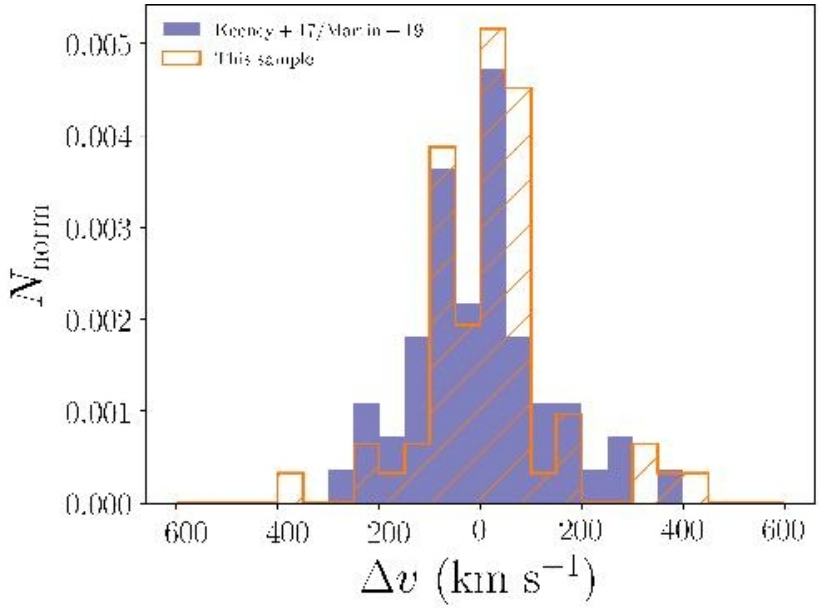

Figure 2. Orange-hatched histogram: velocity distribution of all the 62 Lyα components identified in the 41 QSO spectra in our sample. Purple histogram: velocity distribution of the cool CGM for a subsample of star-forming galaxies with stellar masses consistent with our main sample, drawn from (Keeney et al. 2017; Martin et al. 2019).

…в рамках таких вот моделей

(1)	(2)	(3)	(4)	(5)	(6)	(7)	(8)	(9)	(10)
Model name	M_* range	n_{obj}	$\log(M_*/M_\odot)$	z	SFR ($M_\odot$ yr^{-1})	R_d (kpc)	$\log(M_{vir}/M_\odot)$	r_{vir} (kpc)	T_{vir} (10^6 K)
Gal1	$9.9 \leq \log(M_*/M_\odot) < 10.3$	17	10.1	0.1661	2.60	2.53	11.9	228	0.58
Gal2	$10.3 \leq \log(M_*/M_\odot) < 10.6$	14	10.4	0.0454	1.99	2.65	12.1	286	0.74
Gal3	$10.6 \leq \log(M_*/M_\odot) < 11.0$	10	10.7	0.0425	3.16	3.82	12.3	331	0.98

Table 2. Properties of the 3 galaxy models described in Section 3.1.2. (1) Model name; (2) range in stellar mass; (3) number of galaxies per subsample; (4) median stellar mass; (5) median redshift; (6) median star formation rate; (7) median stellar disc length; (8), (9) and (10) median galaxy virial mass, radius and temperature (see text and Afruni et al. 2019).

Облака выбрасываются из диска by SN и тормозятся горячим газом

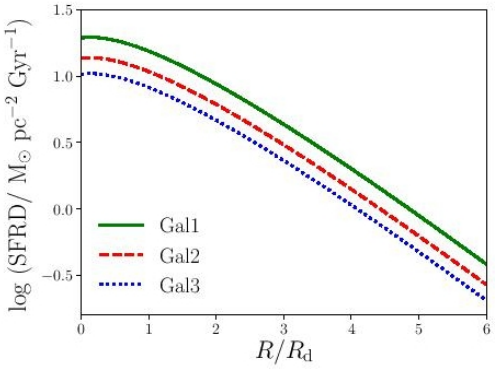

Figure 3. Star formation rate density for the three galaxy models described in Section 3.1.2, derived following Pezzulli et al. (2015).

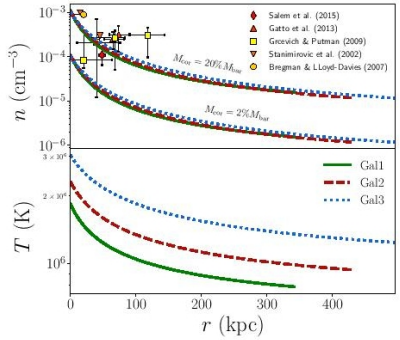

Figure 4. Properties of the hot gas medium for the three galaxy models, respectively density profiles on the top panel and temperature profiles on the bottom panel. The profiles are obtained as described in Section 3.1.3. On the top panel we show both the profiles for a corona bearing 20% and 2% of the total baryonic mass expected within the galaxy halo (see main

We define the corona as a gas in hydrostatic equilibrium with the dark matter halo described by equation (2). More in detail, the hot gas density profile is described by (Binney et al. 2009)

$$\frac{n_e(r)}{n_{e,0}} = \left(\frac{T}{T_0}\right)^{1/(\gamma-1)} , \tag{4}$$

where

$$\frac{T(r)}{T_0} = \frac{\gamma-1}{\gamma}\frac{\mu m_p}{k_B T_0}\left(\Phi(r) - \Phi_0\right) . \tag{5}$$

Here, $\Phi(r)$ is the NFW potential, m_p is the proton mass, $\mu = 0.6$ is the mean molecular weight, γ is the polytropic index and T_0, $n_{e,0}$ and Φ_0 are respectively the temperature, the density and the potential at the reference radius $r_0 = 10$ kpc. The polytropic index and the two normalization factors are chosen in order to have temperature and density profiles consistent with the (uncertain) observational constraints (see Figure 4, where the observational data points are taken from Sormani et al. 2018). More in detail, we use $\gamma = 1.2$, which allows the coronal temperature to vary

The main effect of the hot gas on the clouds is to slow them down by means of the drag force, given by (see Marinacci et al. 2011; Afruni et al. 2019)

$$\dot{v}_{drag} = -\frac{\pi r_{cl}^2 \rho_{cor} v^2}{m_{cl}} , \tag{6}$$

where v is the relative velocity between the clouds and the corona, m_{cl} is the cloud mass, r_{cl} is the cloud radius (set by the choice of the mass and the pressure equilibrium, see Afruni et al. 2019) and $\rho_{cor} = \mu m_p n_{cor}$ is the hot gas mass density, with $\mu = 0.6$ and $n_{cor} = 2.1 n_e$. More massive clouds will be less affected by the in-

В потенциале диска+гало считаются несколько десятков орбит

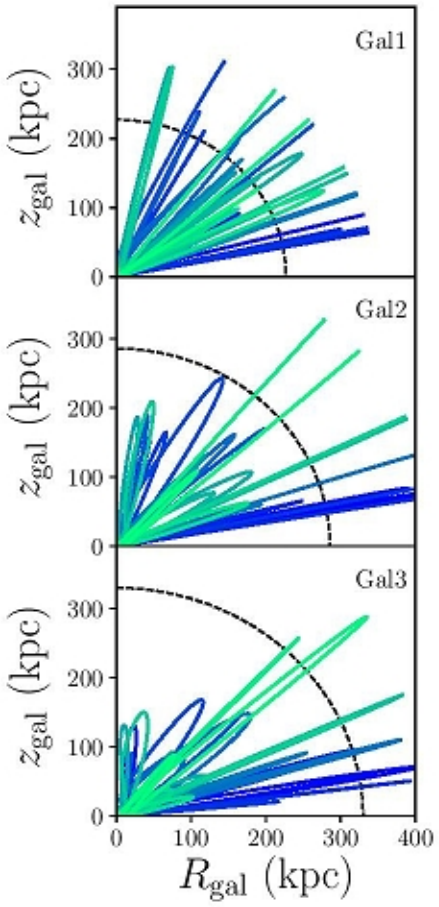

Figure 10. Representative orbits of the clouds for the best models, obtained using the median value of the 4 paramaters reported in Figure 8. The three panels show the results of Gal1,Gal2 and Gal3 and the dashed curves show the value of the virial radius for each of the three galaxies. As in Figure 5, different orbits show different colors.

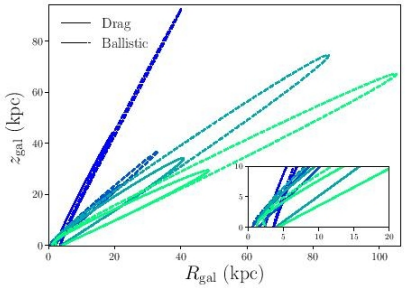

Figure 5. Example of cloud orbits for the model Gal2, with the following choice of parameters: $v_{kick} = 370$ km s^{-1}, $\theta_{max} = 60°$ and $m_{cl} = 10^{6.5}$ $M_\odot$. The dashed lines represent the prediction of a ballistic model, while the solid ones show the effects of the inclusion of the drag force. The colors represent orbits starting from different positions along the galactic disc and with different angles with respect to the z_{gal} axis, selected in the range from 0 to θ_{max}. Small panel: zoom-in on the central region of the halo.

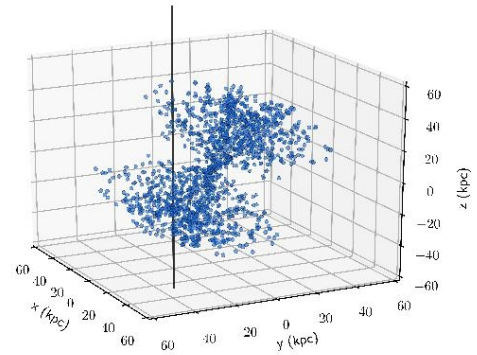

Figure 6. Cloud population for the same model used to create Figure 5, with $\eta = 2$ and a disc inclination $i = 30°$. The clouds are outflowing from the galaxy in a biconical shape. The black line represents one of the lines of sight that we used to perform our synthetic observations.

Как сравнить с наблюдениями: развернуть модель для каждой галактики

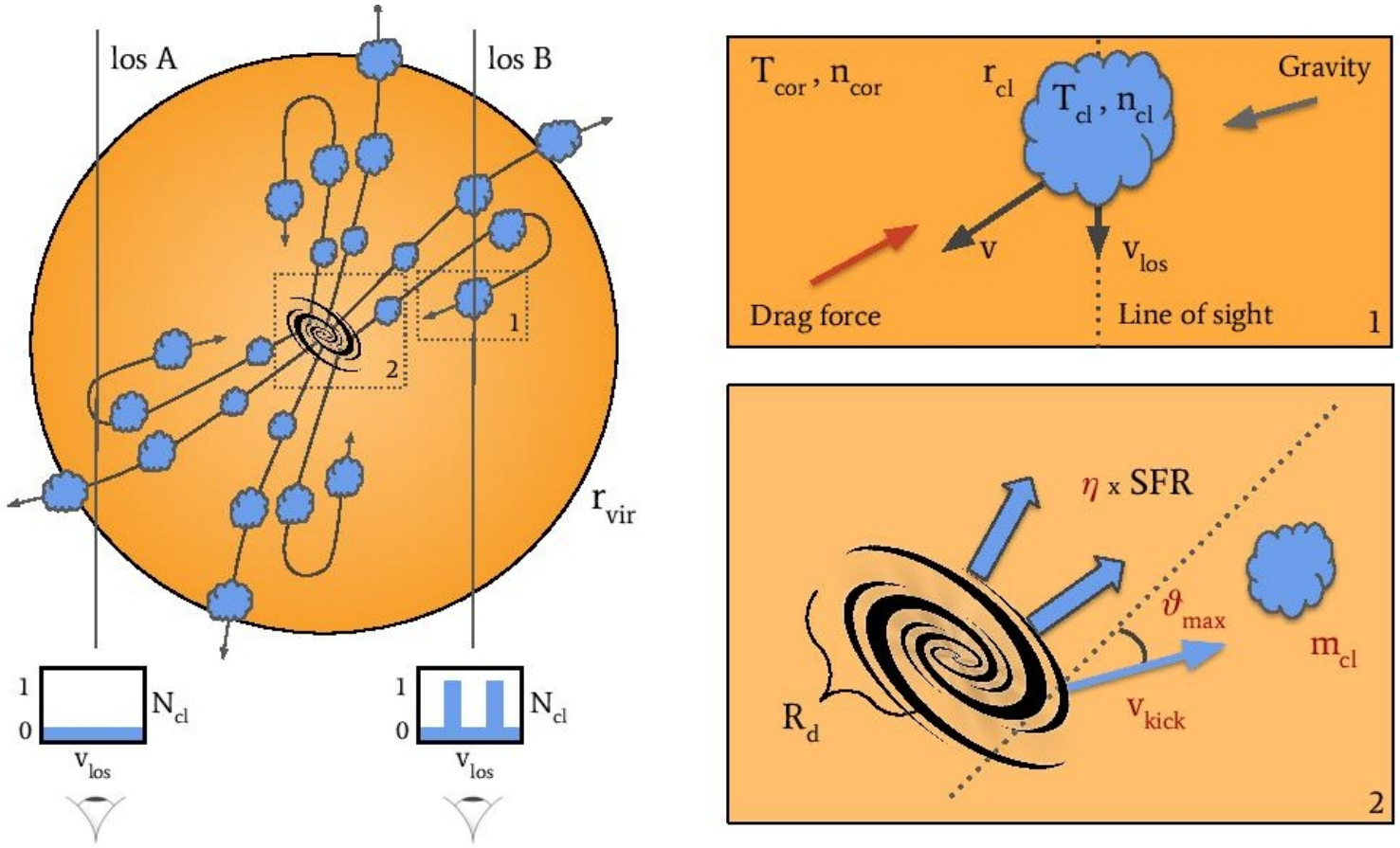

Figure 7. Diagram summarizing the modeling used in this work and described in Section 3. Left diagram: representation of the biconical outflow of clouds

Диапазон варьирования параметров модели

4.1 MCMC analysis

We explored the 4-dimensional parameter space over the following ranges:

- $5 < \log(m_{\rm cl}/M_\odot) < 9$,
- $2 < \log(v_{\rm kick}/({\rm km\ s^{-1}})) < 4$,
- $-2 < \log\eta < 2$,
- $\log 20^\circ < \log\theta_{\rm max} < \log 90^\circ$,

using flat priors for all the parameters in the logarithmic space. In Figure 8 we report the one and two dimensional projections of the posterior distributions for the four parameters, with the values of the 32th, 50th and 68th percentiles (also reported in Table 3). Note from Figure 8 that there is a very well defined region of the parameter space where the posterior is maximized: the models with this choice of parameters represent the physical scenario that best reproduces the observations.

Нашли наилучшие 4 параметра

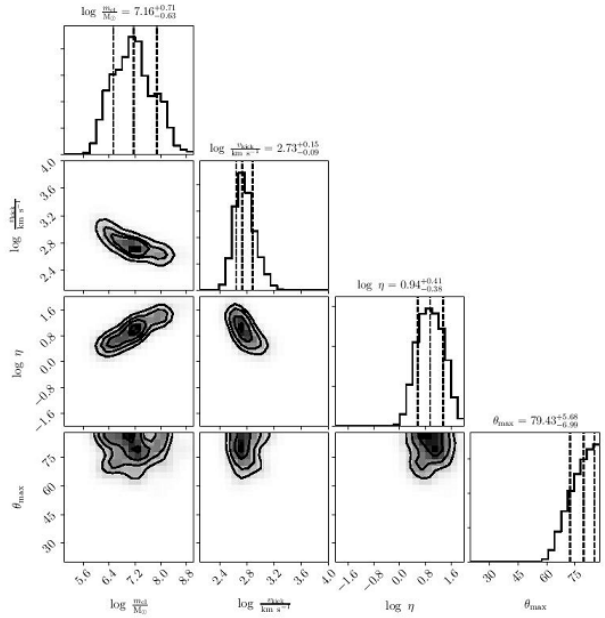

Figure 8. Corner plot with the MCMC results, representing the one and two dimensional projections of the posterior probabilities for the four free parameters of our models. The parameter space is explored in the logarithm of the angle θ_{max}, but the results are transformed here in physical units for clarity.

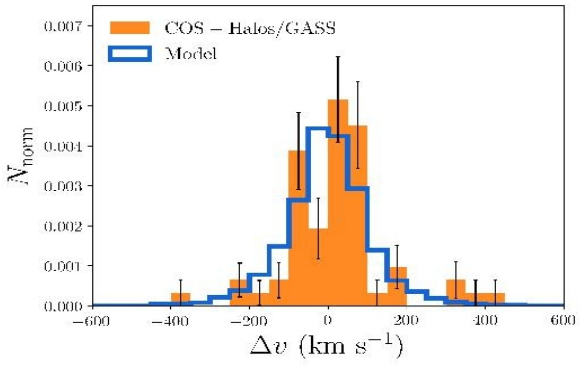

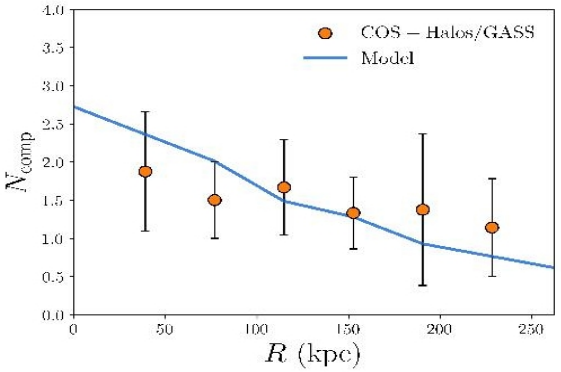

Модель фонтанов не проходит – значит, аккреция!

4.2 Physics of the outflows

In Section 4.1 we have seen that outflow models of cool clouds can reproduce the COS-Halos and COS-GASS kinematic data. In this section we look instead at the implications that this model would have for the efficiency of star formation feedback. The value of the 4 parameters has very important implications from an energetic point of view. The kinetic energy produced by supernovae per unit time and available for the wind is given by (Cimatti et al. 2019)

$$\dot{K} \approx 3 \times 10^{40} \left(\frac{f_{\rm SN}}{0.1}\right) \left(\frac{E_{\rm SN}}{10^{51}\ {\rm erg}}\right) \left(\frac{\rm SFR}{M_\odot\ {\rm yr}^{-1}}\right)\ {\rm erg\ s}^{-1}, \qquad (13)$$

where $f_{\rm SN}$ is the efficiency of the supernovae in transferring energy to the wind and $E_{\rm SN}$ is the amount of energy released by one supernova explosion. We can estimate the efficiency predicted by our models by calculating the kinetic power of the outflowing wind, which can be expressed as

$$\dot{K}_{\rm out} = \frac{1}{2} \dot{M}_{\rm out}\, v_{\rm kick}^2\,, \qquad (14)$$

where $\dot{M}_{\rm out}$ is the mass outflow rate as defined in equation (7). The efficiency necessary to reproduce the cool CGM clouds with our outflow models will then be given by the ratio between equations (13) and (14). Using as a kick velocity and as a mass loading factor the best values found with the MCMC analysis and the canonical value $E_{\rm SN} = 10^{51}$ erg, we obtain $f_{\rm SN} \sim 2.5$, which corresponds to an efficiency of energy transfer from the supernova explosions to the gas wind of about 250%. Clearly, such a value is not physically justifiable, since it means that the outflows would need more energy than the one available from the supernovae. Moreover, from a the-